ISSN 0031-918X, Physics of Metals and Metallography, 2018, Vol. 119, No. 2, pp. 180–190. © Pleiades Publishing, Ltd., 2018.
Original Russian Text © V.A. Shabashov, A.V. Makarov, K.A. Kozlov, V.V. Sagaradze, A.E. Zamatovskii, E.G. Volkova, S.N. Luchko, 2018, published in Fizika Metallov i Metallovedenie, 2018, Vol. 119, No. 2, pp. 193–204.

STRENGTH AND PLASTICITY

Deformation-Induced Dissolution and Precipitation of Nitrides in Austenite and Ferrite of a High-Nitrogen Stainless Steel

V. A. Shabashov[a, *], A. V. Makarov[a, b, c], K. A. Kozlov[a], V. V. Sagaradze[a], A. E. Zamatovskii[a], E. G. Volkova[a], and S. N. Luchko[a]

[a] *Mikheev Institute of Metal Physics, Ural Branch, Russian Academy of Sciences, ul. S. Kovalevskoi 18, Ekaterinburg, 620108 Russia*

[b] *Institute of Engineering Science, Ural Branch, Russian Academy of Sciences, ul. Komsomolskaya 34, Ekaterinburg, 620049 Russia*

[c] *Ural Federal University, ul. Mira 19, Yekaterinburg, 620002 Russia*

**e-mail: shabashov@imp.uran.ru*

Received June 13, 2017; in final form, September 5, 2017

Abstract—Methods of Mössbauer spectroscopy and electron microscopy have been used to study the effect of the severe plastic deformation by high pressure torsion in Bridgman anvils on the dissolution and precipitation of chromium nitrides in the austenitic and ferritic structure of an $Fe_{71.2}Cr_{22.7}Mn_{1.3}N_{4.8}$ high-nitrogen steel. It has been found that an alternative process of dynamic aging with the formation of secondary nitrides affects the kinetics of the dissolution of chromium nitrides. The dynamic aging of ferrite is activated with an increase in the deformation temperature from 80 to 573 K.

Keywords: nitrogen, nitrides, stainless steel, mechanical alloying, dynamic aging, Mössbauer spectroscopy

DOI: 10.1134/S0031918X18020096

INTRODUCTION

The development of nitrogen-containing steels of ferritic and austenitic types is a topical direction of modern metal science of high-strength materials [1–3]. New corrosion-resistant stainless steels of Fe–Cr–N and Fe–Cr–Mn(Ni)–N systems are promising materials [1, 2]. In relation to the improvement of severe plastic deformation methods (equal-channel angular pressing, hydroextrusion, frictional action, treatments in ball mills, etc.), the modification of the structure of steels using large plastic deformation is widely studied [4–10]. In particular, the mechanical alloying of steels with nitrogen was performed using different methods of mechanoactivation [7–10].

Under the conditions of large plastic deformation, cyclic phase transitions, including both the deformation-induced dissolution of nitrides, carbides, oxides, and intermetallic compounds in the metallic matrix and the precipitation of secondary strengthening phases are observed in the structure of alloys and steels [11, 12]. Upon comparing different methods of severe plastic deformation, the effect of the enhanced local temperatures during treatment in the ball mill has been found [13, 14] and the effect of the temperature and rate of deformation upon torsion in Bridgman anvils on the mechanism and kinetics of the mechanical synthesis (MS) in the aging Fe–Ni–*M* alloys has been confirmed [15, 16]. It has been shown that the MS associated with the dissolution of intermetallic compounds upon the cold plastic deformation of alloys is accompanied by processes of dynamic aging, which lead to the formation of second-phase particles, which strengthen the metallic matrix [16, 17]. It is known that nitrogen as an interstitial element has a high chemical activity and a high diffusion mobility even at temperatures below room temperature [18]. In connection with this, the studies of the processes of low-temperature dynamic aging of nitrogen-containing steels under conditions of megadeformation are of great interest.

The present paper is aimed at the study of structural and phase transitions and of the diffusion redistribution induced by severe plastic deformation (in Bridgman anvils) of nitrogen and chromium in the matrix of austenite and ferrite of the high-nitrogen steel with the estimation of the effect of the deformation temperature on this process.

EXPERIMENTAL

As the material for study, an $Fe_{71.2}Cr_{22.7}Mn_{1.3}N_{4.8}$ high-nitrogen hot-deformed steel was used. The chemical composition of this steel is presented in Table 1. The steel was cast under gaseous nitrogen counterpressure. Samples with dimensions of 5.5 × 5.5 × 61.0 mm were quenched from 1453 K in water to

obtain an austenitic structure. Some samples after quenching was subjected to aging at a temperature of 823 K for 0.5 h to stimulate the precipitation of dispersed nitrides in the austenitic matrix. The other part of samples after quenching was aged at the temperature of 923 K for 2.5 h to ensure a more complete decomposition and to destabilize austenite with the precipitation of nitrides and the formation of ferrite upon cooling to room temperature. To study processes of deformation using shear under pressure in Bridgman anvils, i.e., high-pressure torsion, (HPT), samples with dimensions of 5.5 × 5.5 × 0.75 mm were cut using an electric spark machine and were thinned by grinding and electrolytically polishing to a thickness of ~0.65 mm. The samples in the austenitic state after aging at 823 K were deformed at room temperature. The samples in the ferritic state, which were preliminarily aged at 923 K, were deformed at temperatures of 80, 293, 473, and 573 K. Figure 1 shows the schematic of the experiment. To achieve a temperature of 80 K, the anvils with the sample were placed into a container with liquid nitrogen. At first, the samples in the Bridgman anvils were brought to the required temperature, which took 10–20 min. Then, at the selected temperature, the samples were subjected to a pressure of 8 GPa and the shear was performed by rotating the bottom anvil. Depending on the treatment regime, the time of deformation by torsion was 1–10 min. After shear, the sample was returned to room temperature and unloaded. After treatment, the sample was disk-shaped with a thickness of 150 μm and a diameter of 7 mm. To carry out Mössbauer measurements, the disk was thinned to a thickness of 20 μm. As a spot for transmission of γ quanta, the entire area of the sample was used.

Table 1. Elemental composition of the $Fe_{71.2}Cr_{22.7}Mn_{1.3}N_{4.8}$ steel

	Fe	Cr	Mn	N	C
wt %	75.0	22.2	1.38	1.24	0.08
at %	71.2	22.7	1.33	4.78	0.36

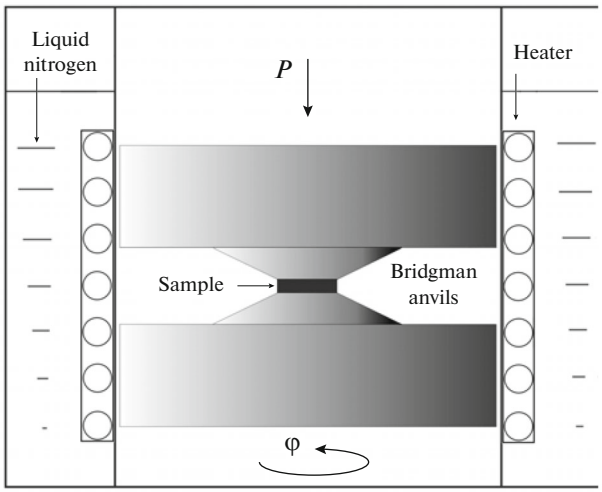

Fig. 1. Scheme of deformation by HPT in the temperature range of 80–573 K.

The degree of true strain upon HPT was estimated according to the following formula [16]:

$$\varepsilon = \varepsilon_{com} + \ln\left(1 + \frac{\phi^2 r^2}{d^2}\right)^{1/2}, \quad (1)$$

where ε_{com} is the deformation by compression; $\phi = k \times 2\pi$ is the angle of rotation of the anvils upon shear, where k is the number of revolutions; r is the distance from the sample center to the investigated region; and d is the thickness of the sample after deformation. The degree of deformation ε, which was determined using formula (1), was estimated as the average value taking into account the area of the sample with a certain radius r. The regimes of deformation action are shown in Tables 2 and 3.

The Mössbauer spectra of the absorption of γ quanta with an energy of 14.4 keV at ^{57}Fe were obtained from a Co(Cr) source at room temperature in the constant-acceleration regime. The same samples were used for studies based on the method of thin foils using a JEM-200CX transmission electron microscope.

Table 2. Parameters of spectra and the nitrogen content x(N) in austenite of the $Fe_{71.2}Cr_{22.7}Mn_{1.3}N_{4.8}$ steel after quenching, aging, and HPT at 8 GPa, ε = 5.7 (3 rev) at room temperature

Treatment	Parameters											
	M			D0				D1				x(N) at % ±0.4
	I_S, mm/s ±0.01	Γ, mm/s ± 0.02	A, %	I_S, mm/s ±0.01	Q_S, mm/s ±0.02	Γ, mm/s ±0.02	A, % ± 2	I_S, mm/s ±0.01	Q_S, mm/s ±0.02	Γ, mm/s ±0.02	A, % ±2	
Quenching	–0.10	0.22	25	–0.08	0.22	0.24	60	–0.05	0.48	0.21	15	2.5
Aging at 823 K	–0.09	0.20	25	–0.09	0.22	0.24	64	–0.04	0.48	0.22	11	1.7
Aging at 823 K + HPT	–0.10	0.21	23	–0.08	0.21	0.24	55	–0.04	0.48	0.22	22	3.7

Table 3. Dependence of $\langle H \rangle$ and chromium content x(Cr) in the α phase of the $Fe_{71.2}Cr_{22.7}Mn_{1.3}N_{4.8}$ steel after aging at 923 K and subsequent HPT at 8 GPa, ε = 5.1 (2 rev) at different temperatures

Calculation formula	Treatment					
	parameters	aging, 2.5 h	HPT at 80 K	HPT at 293 K	HPT at 473 K	HPT at 573 K
Formula (6)	$\langle H \rangle$, kOe ± 1	284	276	281	282	285
	x(Cr), at % ± 0.5	18.5	21.9	19.8	19.3	18.0
Formula (4)	x(Cr), at % ± 1	16	20	17	16	16

The calculation of the Mössbauer spectra was carried out using special software (MS Tools) [19]. The calculation involved reconstructing the distribution of hyperfine magnetic fields $p(H)$ and the distribution of the gravity centers of singlet (apparatus) lines on the scale of Doppler velocities $p(V)$ using the regulation method. Then, the $p(H)$ and $p(V)$ distributions were used to simulate and approximate experimental spectra by the sum of several subspectra that correspond to different nonequivalent surroundings of ^{57}Fe atoms.

RESULTS

The structural and phase transitions induced by severe plastic deformation have been studied in two different initial states of the $Fe_{71.2}Cr_{22.7}Mn_{1.3}N_{4.8}$ aged steel, i.e., austenite and ferrite with decomposition products in the form of chromium nitrides Cr_2N (CrN).

Aging of $Fe_{71.2}Cr_{22.7}Mn_{1.3}N_{4.8}$ Steel

Austenite with decomposition products in the form of nitrides was obtained by aging the quenched steel at 823 K for 0.5 h. In the austenite structure, individual coarse particles of Cr_2N nitrides are present with sizes of ~0.5 μm, which remained undissolved after heating for quenching [20]. As a result of aging at 823 K, new fine crystals of CrN nitrides are precipitated in the austenite matrix (Figs. 2a, 2b). After quenching, the

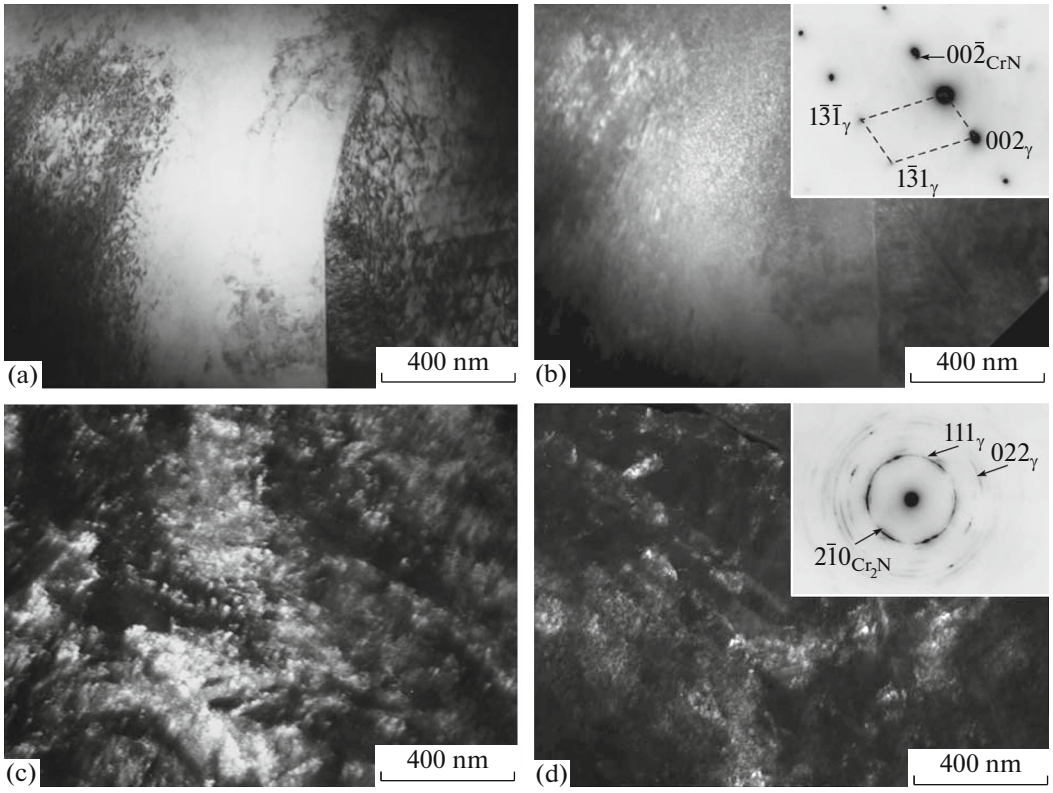

Fig. 2. Structure of the $Fe_{71.2}Cr_{22.7}Mn_{1.3}N_{4.8}$ steel quenched from 1453 K after (a, b) aging at 823 K for 0.5 h and (c, d) subsequent deformation by HPT: (a) bright-field image; (b) dark-field image in the $00\bar{2}_{CrN}$ reflection; zone axis $[130]_\gamma$; (c) dark-field image in the 111_γ reflection; (d) dark-field image in the $2\bar{1}0_{Cr_2N}$ reflection and electron-diffraction pattern.

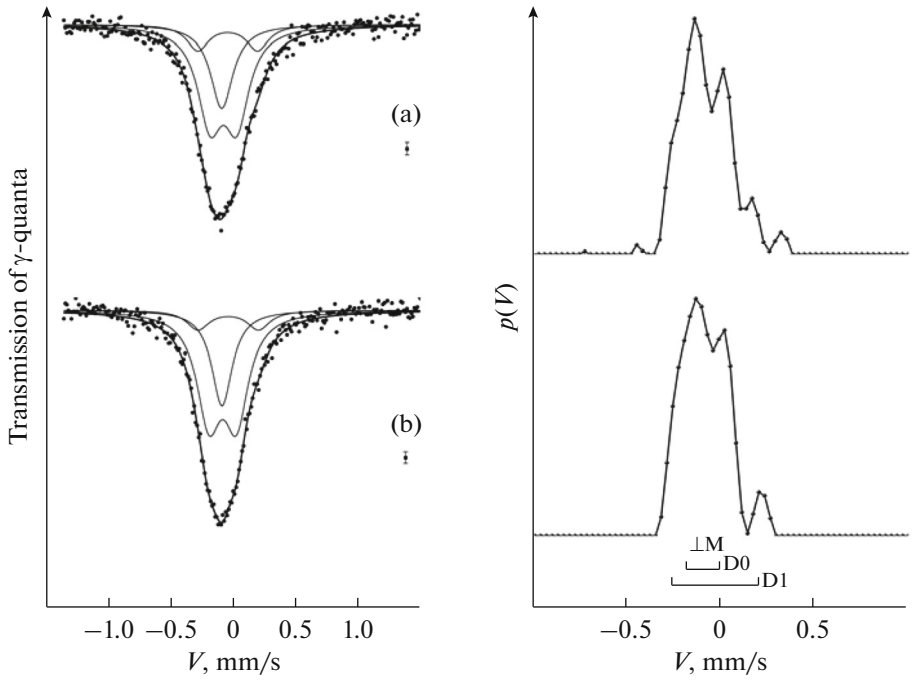

Fig. 3. Mossbauer spectra and $p(V)$ functions of the $Fe_{71.2}Cr_{22.7}Mn_{1.3}N_{4.8}$ steel. Treatment: (a) water quenching from 1453 K after holding for 1 h; (b) water quenching from 1453 K after holding for 1 h + aging at 823 K for 0.5 h.

steel is paramagnetic and its Mössbauer spectrum represents an asymmetric singlet with an enhanced width (Fig. 3a). The reason for the broadening is the presence of substitutional (Cr, Mn) and interstitial (N) impurity atoms in the surroundings of the resonant iron atoms. According to [10, 21–23], the main reason of the broadening is associated with the distribution of the electric-field gradient (EFG) at the iron atoms. To improve the resolution of the austenite spectra, the procedure for reconstruction $p(V)$ was carried out [10, 19]. The results of approximating the spectrum using Lorentzian forms make it possible to propose a model for describing the spectrum in the form of a superposition of components M, D0, and D1 with parameters presented in Table 2. The singlet line M is hypothetically caused by the part of the metallic matrix that does not contain atoms of chromium, magnesium, and nitrogen in the nearest surroundings of ^{57}Fe. The values of the quadrupole splitting and isomer shift of the doublet D0 are close to the hyperfine parameters of the stainless steel [21]. In addition to substitutional elements (Cr and Mn), its formation can be explained by the presence of nitrogen in the second coordination shell (CS) of the octahedral interstices [23]. The doublet D1 has hyperfine parameters that are close to the parameters of the doublet of nitrogen interstitials in the first CS of the octahedral interstices of fcc iron [24]. The spectrum calculated using the model of three components (with the following parameters: isomer shift I_s, quadrupole splitting Q_s, width of the Lorentzian lines Γ, and integral intensity A) is in good agreement with the experimental spectrum (Table 2). The nitrogen content x(N) in the solid solution of the quenched austenite γ-FeN was estimated under the assumption of repulsive distribution (mutual repulsion of nitrogen atoms) [2, 24] based on the contribution of configurations from iron atoms with a single nitrogen atom in the nearest octahedral interstices S_{D1} according to the following formula [24]:

$$S_{D1} = 6p(1 - p). \quad (2)$$

Here, $p = x/(1 - x)$ is the fraction of octahedral interstices in austenite that are occupied by nitrogen.

According to the experimental data, aging at 823 K according to (2) leads to a decrease in the nitrogen content in the γ solid solution from 2.5 (in the quenched state) to 1.7 at % (Table 2).

The ferrite of the $Fe_{71.2}Cr_{22.7}Mn_{1.3}N_{4.8}$ steel with decomposition products was obtained after aging at 923 K for 2.5 h, which leads to a depletion of nitrogen of the austenite and a decrease in its stability upon cooling (in water) to room temperature. Figure 4 shows the structure of the steel after aging at 923 K for 2.5 h. As a result of the $\gamma \rightarrow \alpha$ transformation, there is formed a pearlite-like structure consisting of extended elongated grains or whole packets of ferrite grains (Fig. 4a) and thin interlayers of Cr_2N nitride, which shinet in the dark-field image taken in the nitride reflection (Fig. 4b). No structures with equiaxed nitrides have been detected.

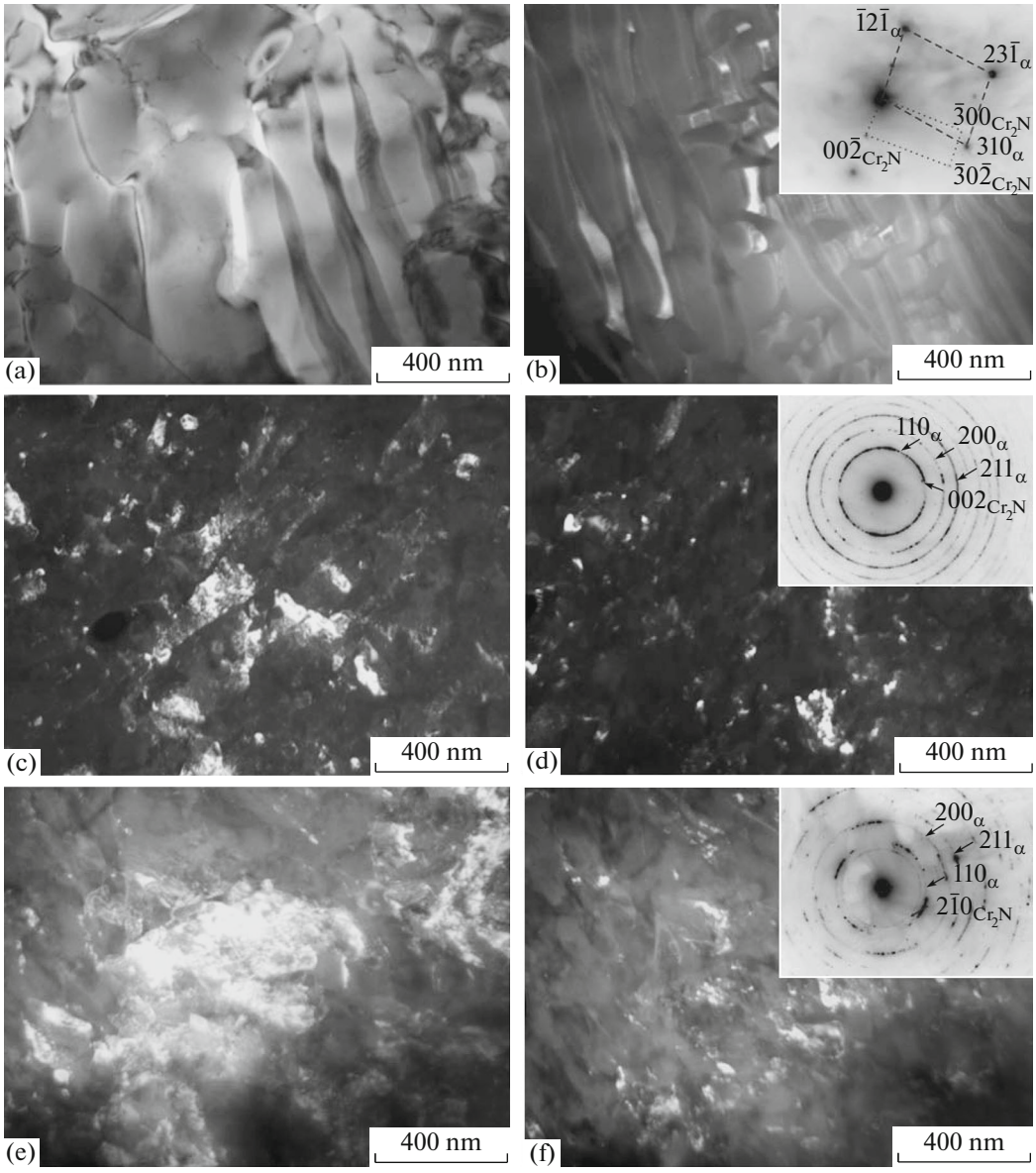

Fig. 4. Structure of the $Fe_{71.2}Cr_{22.7}Mn_{1.3}N_{4.8}$ steel quenched from 1453 K after (a, b) aging at 923 K for 2.5 h and subsequent deformation by HPT (c, d) at 923 K and (e, f) at 573 K: (a) bright-field image; (b) dark-field image in the $00\bar{2}_{CrN}$ reflection and electron-diffraction pattern (zone axes $[\bar{1}37]_\alpha$ and $[010]_{Cr_2N}$); (c) dark-field image in the 110_α reflection; (d) dark-field image in the $2\bar{1}0_{Cr_2N} + 110_\alpha$ reflection and electron-diffraction pattern (Cr_2N and bcc rings are indicated by arrows); (e) dark-field image in the 110_α reflection; (f) dark-field image in the $2\bar{1}0_{Cr_2N}$ reflection and electron-diffraction pattern (Cr_2N and bcc rings are indicated by arrows).

The experimental Mössbauer spectrum of the ferrite sample obtained by annealing at 923 K for 2.5 h is a sextet with broadened lines (Figs. 5a, 6a). The view of the spectrum is similar to the spectrum of the α (bcc) solid solution of a binary Fe–Cr alloy of close composition [25]. In the integrated spectrum, sextets are observed, while in the $p(H)$ distribution, there are peaks that correspond to the surroundings of resonant iron atoms with different amounts of chromium impurity atoms in the nearest sites of the bcc lattice [25, 26]. The values of the hyperfine field of the sextets S(n) coincide with the fields characteristic of binary Fe–Cr alloys of close composition [26]:

$$H(n_1, n_2) = H(0,0) + n_1\Delta H_1 + n_2\Delta H_2, \qquad (3)$$

where $H(0, 0)$ is the hyperfine magnetic field at a ^{57}Fe nucleus without chromium atoms in the nearest two CSs; ΔH_1 and ΔH_2 are the changes of the fields that are caused by chromium atoms located in the first and second CSs, respectively; n_1 and n_2 are the amounts of

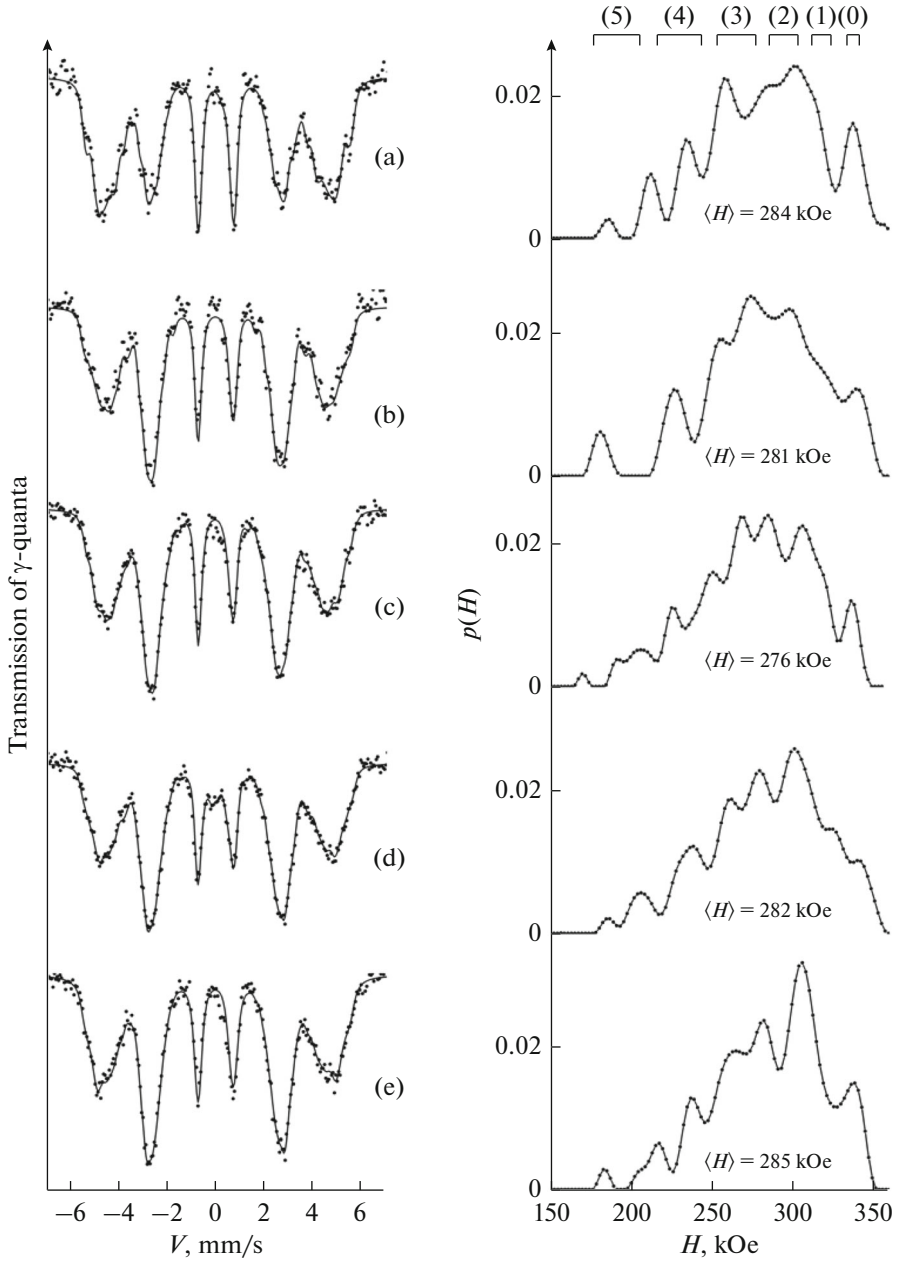

Fig. 5. Mossbauer spectra and $p(H)$ distribution function of the $Fe_{71.2}Cr_{22.7}Mn_{1.3}N_{4.8}$ steel. Treatment: (a) quenching from 1453 K in water and annealing at 923 K for 2.5 h; quenching from 1453 K in water and annealing at 923 K for 2.5 h + HPT (2 rev, 0.3 rev/min, $P = 8$ GPa) (b) at $T = 293$ K; (c) at $T = 80$ K; (d) at $T = 473$ K; (e) at $T = 573$ K.

chromium atoms in the first and second nearest CSs of iron atoms.

Taking into account the similarity of the two CSs and of the values of the disturbances ΔH_1 and ΔH_2, the integrated spectra of Fe–Cr alloys can be approximated by the superposition of sextets corresponding to the atomic configurations with n chromium atoms in the nearest two CSs without their separation. The partial contributions from the sextets S(n) are proportional to the probability $W(n)$ of the occurrence of n chromium atoms in the nearest two CSs of iron. The separation of the partial contributions of the sextets makes it possible to estimate the effective chromium concentration in the aged bcc solid solution and after deformation according to the following relation:

$$x(Cr) = \sum_{n}^{z_1+z_2} n W(n) / z_1 + z_2, \quad (4)$$

where $n = n_1 + n_2$; $z_1 = 8$, $z_2 = 6$ for the first and second CSs. The $p(H)$ distribution (Fig. 5a) shows the ranges of effective magnetic fields. In Fig. 6a, the sextets that

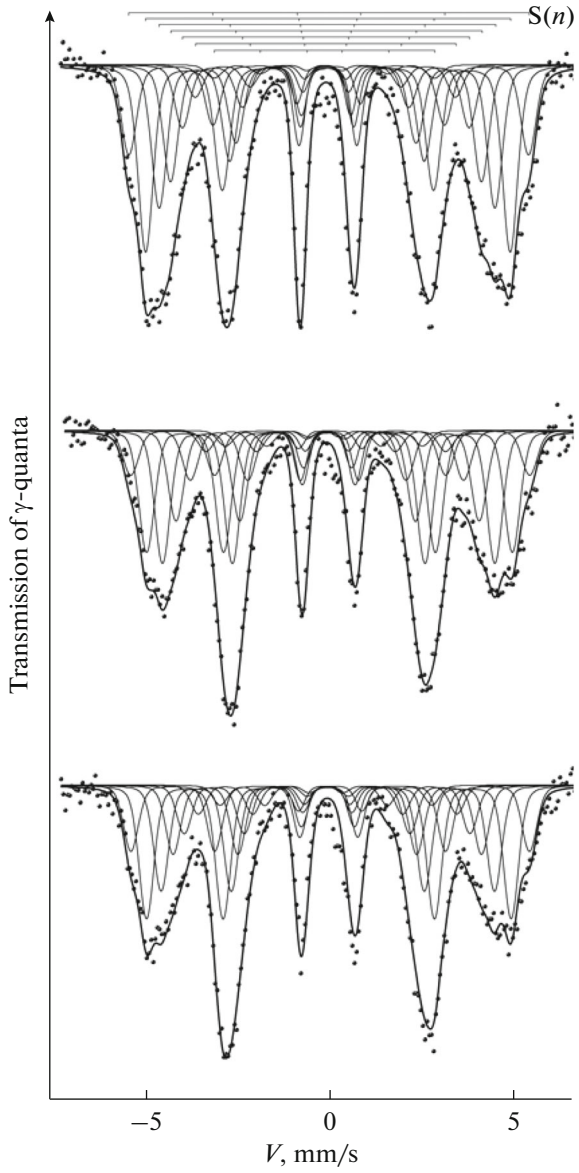

Fig. 6. Calculation of Mössbauer spectra of $Fe_{71.2}Cr_{22.7}Mn_{1.3}N_{4.8}$ steel with resolution of subspectra S(n) corresponding to configurations with n chromium atoms in the first two CSs of ^{57}Fe atoms. Treatment: (a) quenching from 1453 K in water and annealing at 923 K for 2.5 h; quenching from 1453 K in water and annealing at 923 K for 2.5 h + SP (2 rev, 0.3 rev/min, P = 8 GPa) (b) at T = 80 K; (c) at T = 573 K.

correspond to n(0, 1, 2, etc.) Cr impurity atoms in the nearest two CSs relative to iron are indicated. To describe the lines of sextets S(n), the modified Lorentzian form with the same width was chosen. The neglect of the overlap of fields from atomic configurations with an increased impurity content leads to an underestimation of the values of x(Cr). The verification of the proposed estimate of x(Cr) was performed on binary Fe–Cr alloys using the comparison of the results of the theoretical calculation of $W(n)$ with the results of the approximation of the spectrum by sextets [25, 26].

Apart from the direct calculation of x(Cr), data on the connection between the chromium content in bcc Fe–Cr alloys and the average hyperfine magnetic field were used. According to [25], the dependence of $\langle H\rangle$ on the chromium content x(Cr) in the solid solution is linear:

$$\langle H\rangle = 330 - 230.1\times x(\mathrm{Cr}). \quad (5)$$

Manganese that is present in the steel (~1.33 at %), just as chromium, can lead to a decrease in $\langle H\rangle$ [28, 29]. The effect of the insignificant amount of manganese can be taken into account as a fixed additive in $\langle H\rangle$. According to [28], this contribution ΔH_{Mn} is estimated as −3.5 kOe. Then, the $\langle H\rangle$ dependence on the chromium content in the steel is described as follows:

$$\langle H\rangle = 330 + \Delta H_{\mathrm{Mn}} - 230.1\times x(\mathrm{Cr}). \quad (6)$$

The presence of nitrogen in the state of the solid solution in bcc Fe–Cr–N has only an insignificant effect on $\langle H\rangle$ [11].

Aging at 923 K for 0.5 and 2.5 h leads to the partial and complete disappearance, respectively, of the austenite singlet in the spectrum of the steel (Fig. 5a). The increase in $\langle H\rangle$ of the sextet of the α phase from 282 to 284 kOe with an increase in the aging time from 0.5 to 2.5 h at 923 K indicates a decrease in the chromium content in the matrix and confirms its escape from the matrix into the chromium nitrides [28, 29].

ROOM-TEMPERATURE HIGH-PRESSURE TORSION OF AGED $Fe_{71.2}Cr_{22.7}Mn_{1.3}N_{4.8}$ STEEL

HPT at 8 GPa with ε = 5.7 (3 rev) of Austenite Aged at 823 K for 0.5 h

Figures 2c and 2d show the structure of austenite deformed by HPT. It can be seen that, as a result of HPT, submicrocrystalline austenite is formed in a mixture with nanosized nitrides. The relative intensity of the D1 doublet increases by 11% in the Mössbauer singlet of the deformed sample, which, according to the formula (2), corresponds to an increase in the nitrogen content in the γ solid solution to 3.7 at % (Fig. 7, Table 2). In addition, after HPT, additional third and fourth lines of the sextet of the α phase appear.

HPT at 8 GPa with ε = 5.1 (2 rev) of Ferrite Aged at 923 K for 2.5 h

Figures 4c and 4d show electron-microscopic images of the structure of ferrite deformed by HPT. It can be seen that a dispersed submicrocrystalline structure is formed, which contains both fine (up to several nanometers) crystallites and coarse crystalline fragments of submicron sizes (Fig. 4c). The electron-dif-

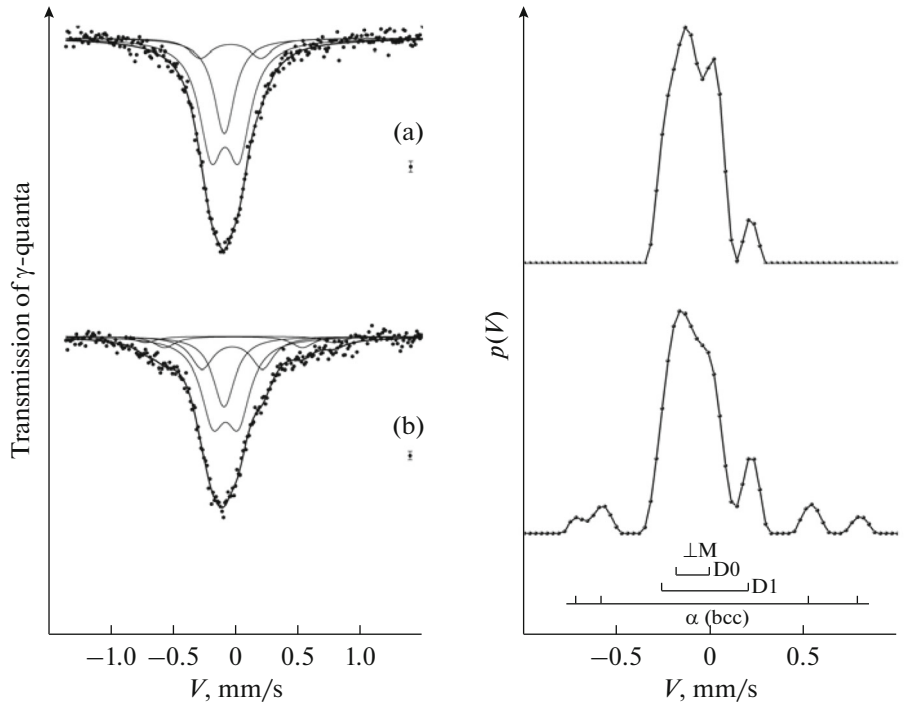

Fig. 7. Mössbauer spectra and $p(V)$ functions of the $Fe_{71.2}Cr_{22.7}Mn_{1.3}N_{4.8}$ steel. Treatment: (a) aging at 823 K for 0.5 h; (b) aging at 823 K for 0.5 h + HPT (3 rev, 0.3 rev/min, $P = 8$ GPa) at $T = 293$ K.

fraction patterns contain discontinuous rings (Fig. 4d). In the electron-microscopic images, an elongation of grains is observed, and the formation of dislocation cellular and banded structures occurs. The electron-diffraction patterns in the form of nonuniform rings and the relatively small contrast between bright and dark regions in the bright-field images indicate the predominance of low-angle misorientations between ferrite subgrains. Because of a close location of the Cr_2N reflection near the 110_α ring, the dark-field image upon the dark-field analysis in the nitride reflection is in fact obtained in the complex 110_α + Cr_2N (Fig. 4d) reflection. The coarser elongated crystals belong to the α phase; the fine particles located predominantly along the boundaries of extended coarse crystals are dispersed nitrides formed as a result of the fragmentation of the Cr_2N coarse nitrides.

In the Mössbauer sextets of ferrite after HPT there is observed a strong magnetic texture caused by the preferential location of magnetic moments in the plane of the sample (Figs. 5, 6). After deformation at 293 K, an increase in the intensity of $p(H)$ peaks in the range of fields of 170–200 kOe occurs owing to a decrease in the intensity in the range of 300–340 kOe (Figs. 5a, 5b). The changes in $p(H)$ are associated with the growth of chromium-rich atomic surroundings of iron atoms (with 4 and 5 chromium atoms) owing to a decrease in the amount of atomic surroundings with 0 and 1 chromium atoms in the nearest CSs of iron atoms. The observed changes in $p(H)$ cause a decrease in $\langle H \rangle$ from 284 to 281 and 279 kOe and, according to the dependence (6), an increase in the effective chromium concentration x(Cr) in the solid solution of the α phase from 18.5 at % in the aged state to 19.8 at % (after HPT 2 rev) and 20.6 at % Cr (3 rev). The direct calculation according to the formula (4) also shows an increase in x(Cr) (Fig. 6; Table 3).

HPT of Ferrite of $Fe_{71.2}Cr_{22.7}Mn_{1.3}N_{4.8}$ Steel in the Temperature Range of 80–573 K

The metallic matrix of the steel before and after deformation to $\varepsilon = 5.1$ (2 rev) in the temperature range of 80–573 K is retained in the α (bcc) modification. The Mössbauer data and concentrations x(Cr) in the solid solution in the α phase after aging and deformation are given in Figs. 5 and 6 and in Table 3. It follows from the spectra and from the $p(H)$ distributions that the changes observed after deformation at 80 K are similar to those after HPT at room temperature. The greatest increase in the contribution from chromium-rich atomic configurations is observed after deformation at 80 K, which leads to a decrease in $\langle H \rangle$ from 284 to 276 kOe (Fig. 5c). The average effective chromium concentration increases to 19.8 and 21.9 at % after HPT at 293 and 80 K, respectively. The analogous data follow from the calculations using relation (4) (Fig. 6; Table 3).

The opposite result is observed upon an increase in the deformation temperature. After HPT at 473 K,

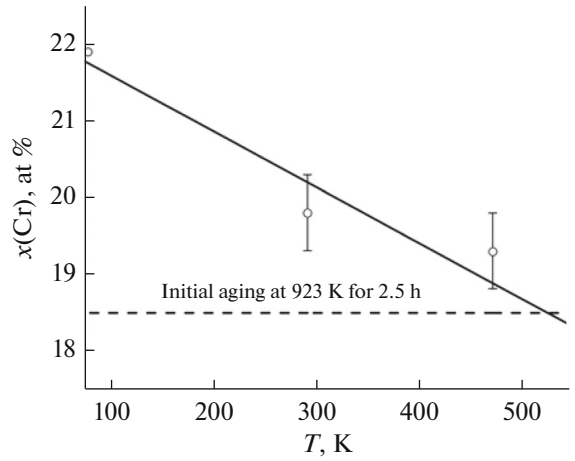

Fig. 8. Dependence of chromium content in matrix of $Fe_{71.2}Cr_{22.7}Mn_{1.3}N_{4.8}$ steel on temperature of deformation by HPT (3 rev, 0.3 rev/min, $P = 8$ GPa).

there is observed an increase in the intensity of $p(H)$ in the range of fields of ~310 kOe, which correspond to the surroundings with a single chromium impurity atom, due to a decrease in the intensity in the range of 170–200 kOe (Figs. 5c, 5d). This tendency is enhanced with an increase in the deformation temperature to 573 K and, according to the dependences (4) and (6), indicates the absence of changes or a decrease in the chromium content in the matrix α phase from 18.5 to 18.0 at % (Figs. 5e, 6c; Table 3). The electron-microscopic data indicate an enhancement of the process of aging under deformation conditions at 573K (Figs. 4e, 4f). The dark-field image shows the formation of a submicrocrystalline structure (Fig. 4e). In the electron-diffraction pattern, there are reflections of the Cr_2N nitride phase in addition to the reflections of the α phase; a $2\bar{1}0_{Cr_2N}$ ring is clearly observed (Fig. 4f). In the electron-microscopic image taken in the nitride reflection, fine particles of nitrides are shining. The morphology of these particles does not differ from the morphology of the nitrides in Fig. 4d, but the amount of nitride particles increases.

DISCUSSION

Under the conditions of cold deformation at room temperature, an increase is observed in the nitrogen content in the state of the interstitial solid solution in the matrix of the aged steel with the austenite structure; in the structure of ferrite, an increase in the chromium content in the substitutional solid solution in the α phase is observed. This indicates the deformation-induced dissolution of chromium nitrides. As a result of HPT at room temperature, in $Fe_{71.2}Cr_{22.7}Mn_{1.3}N_{4.8}$ steel aged at 823 K for 0.5 h the nitrogen content in the austenitic fcc matrix increases by 2 at % (Table 2). It should be noted that the amount of nitrogen in the solid solution in the initial austenite (2.5 at %) is noticeably smaller than the nitrogen concentration specified upon melting (4.8 at %), which is associated with an incomplete dissolution of nitrides during heating for quenching [20]. The increase in the nitrogen content to 3.7 at % in the γ solid solution after deformation at room temperature indicates the deformation-induced dissolution of nitrides. Earlier [10], the deformation-induced dissolution of chromium nitrides formed as the products of the cellular decomposition of the $Fe_{56.9}Mn_{21.5}Cr_{18.6}N_{3.0}$ austenitic steel aged at 1073 K was observed after plastic deformation by sliding friction and HPT in Bridgman anvils. The increase in the nitrogen content in the austenitic matrix was also observed after deformation [10].

The deformation-induced dissolution of chromium nitrides also occurs in the ferritic matrix of the investigated steel. Under similar conditions of deformation by HPT at room temperature, the chromium content in the matrix of the α phase increases from 18.5 to 19.8 and 20.6 at % at $\varepsilon = 5.1$ (2 rev) and $\varepsilon = 5.7$ (3 rev), respectively. It can be assumed that nitrogen enters into the matrix together with chromium (2.1 at %). Taking into account the stoichiometry of the Cr_2N nitride, the alloying of the matrix bcc solid solution with nitrogen in the amount to 1.0 at % occurs. This amount is smaller than that of nitrogen (2 at %) mechanically dissolved in the austenite aged at 823 K after HPT.

To understand the mechanism of the deformation-induced redistribution of nitrogen in the matrix of the steel, the results of the experiments on the effect of the temperature of deformation by HPT on the kinetics of the dissolution of nitrides in the α phase are important (Fig. 8; Table 3). It follows from Mössbauer data that there is a substantial increase in the content of chromium coming from the chromium nitrides into the α phase, i.e., from 18.5 at % in the aged steel to 19.3, 19.8, and 21.9 at % for HPT at temperatures of 473, 292, and 80 K, respectively. This increase can be explained by the weakening of the alternative process of dynamic decomposition of the metastable solid solution supersaturated with nitrogen (deformation-induced dynamic aging [16, 30]), which accompanies the nonequilibrium deformation-induced dissolution of the nitride particles. The occurrence of a thermally activated process of dynamic aging is confirmed by the data on the deformation of the steel at 575 K, which leads to an additional (with respect to the initial state) decrease in the Cr concentration from 18.5 to 18.0 at % (Figs. 5, 8; Table 3). The formation of second-phase particles of chromium nitrides arising as a result of mechanical alloying using mills and upon HPT in Fe–Ni-based nitrogen-containing alloys was shown also in [8].

The data on the nonequilibrium dissolution of nitrides upon a decrease in the deformation temperature from room temperature to cryogenic tempera-

tures are of special interest (Figs. 5b, 5c, 8). In [31, 32], the possibility of the lattice diffusion of nickel was shown in the case when the atoms pass into the interstitial state with a relatively low activation energy of 0.1–0.2 eV. Upon HPT, the transition of atoms into the interstitial positions is caused by the achievement of critical local stresses [5, 33] and by large gradients of stresses [34, 35]. The activity of the relaxation constituent related to aging, which partially compensates the processes of nonequilibrium dissolution of intermetallic particles, is retained up to low temperatures. On the example of the deformation-induced dissolution of $\gamma'(Ni_3M)$ intermetallic particles in the fcc matrix of Fe–Ni–*M* alloys, the strong dependence of the kinetics of the dynamic aging on the temperature and rate of deformation, as well as on the diffusion mobility and chemical activity of the alloying elements was shown in [15–17]. Thus, with a decrease of the deformation temperature to 80 K, a decrease is observed in the diffusion mobility of point defects. However, even at room temperature, the mobility of the interstitial atoms providing the possibility of diffusion in the fields of stresses of moving dislocations is retained [36]. In the present paper, this follows from the data on the increase in the degree of dissolution of chromium nitrides following a decrease in temperature from room temperature to 80 K. The dynamic aging in the high-nitrogen steel under investigation is stimulated by the high chemical activity of the formation of chromium nitrides [29], the generation of a large amount of point defects and by the high diffusion mobility of nitrogen atoms, even below room temperature [2].

CONCLUSIONS

(1) The use of methods of Mössbauer spectroscopy and electron microscopy made it possible to detect processes of the dissolution of chromium nitrides in austenite and ferrite of the $Fe_{71.2}Cr_{22.7}Mn_{1.3}N_{4.8}$ aged high-nitrogen steel, which were induced by the shear deformation under pressure (high-pressure torsion, HPT) in rotating Bridgman anvils.

(2) Under conditions of cold deformation (293 K) by HPT at 8 GPa with a degree of deformation $\varepsilon = 5.7$ (with three revolutions of the anvils (3 rev)), the nitrogen content in the interstitial positions in austenite of the steel preliminarily aged at 823 K increases by 2 at % because of a noneqiulubrium diffusion of nitrogen from nitrides. The total nitrogen content in austenite after deformation exceeds that obtained upon quenching due to the deformation-induced dissolution of chromium nitrides in the austenitic matrix.

(3) In the ferrite of the steel aged at 923 K and containing Cr_2N chromium nitrides, there is an increase in the chromium content in the bcc matrix from the initial values of 18.5 at % to 19.3, 19.8, and 21.9 at % with a decrease in the temperature of the HPT from 473 to 293 and 80 K, respectively, at $\varepsilon = 5.1$ (2 rev) because of the dissolution of chromium nitrides and a decrease in the activity of the competing deformation-induced aging.

(4) An additional decrease or retention of the chromium content in the matrix occurs upon an increase in the deformation temperature to 573 K in the steel preliminarily aged at 923 K for 2.5 h. This fact is explained by an acceleration of the decomposition of the metastable solid solution supersaturated with nitrogen, which leads to a nonequilibrium dissolution of chromium nitrides because of the high diffusion mobility of nitrogen and continuous generation of a high amount of point defects upon megaplastic deformation by HPT.

ACKNOWLEDGMENTS

The authors are grateful to Professor Ts. Rashev for the providing of the material for the study and to Cand. Sci. (Eng.) A. L. Osintseva for the help in the carrying out of the heat treatment of the steel. This work was performed according to the State Task of the Federal Agency of Scientific Organizations of the Russian Federation (theme "Structure," no. 01201463331) and was supported in part by the project of the Ural Branch of the Russian Academy of Sciences (no. 15-9-12-45). Transmission electron microscopic investigations were carried out at the Electronic Microscopy Department of the Center of Collaborative Access Testing Center of Nanotechnologies and Advanced Materials of the Institute of Metal Physics, Ural Branch, Russian Academy of Sciences.

REFERENCES

1. N. P. Lyakishev and O. A. Bannykh, "New structural steels with an overequilibrium content of nitrogen," Perspekt. Mater., No. 1, 73–82 (1995).
2. H. Berns, V. Gavriljuk, and S. Reindner, *High Interstitial Stainless Austenitic Steels* (Springer, Berlin, 2013).
3. Ts. V. Rashev, *High-Nitrogen Steels: Metallurgy under Pressure* (Bolg. Acad. Sci., Sofia, 1995).
4. C. Suryanarayana, Mechanical Alloying and Milling (Marcel Dekker, New York, 2004).
5. D. S. Gertsriken, V. F. Mazanko, V. M. Tyshkevich, and V. M. Fal'chenko, *Mass Transfer in Metals at Low Temperatures under External Actions* (RIO IMF, Kiev, 1999) [in Russian].
6. A. V. Makarov, L. G. Korshunov, V. B. Vykhodets, T. E. Kurennykh, and R. A. Savrai, "Effect of strengthening friction treatment on the chemical composition, structure, and tribological properties of a high-carbon steel," Phys. Met. Metallogr. **110**, 507–521 (2010).
7. A. A. Popovich and V. A. Popovich, "Functioanal powder materials based on nanostructures," in *Functional Powder Materials*: A collection of Papers, (Nauchn. Tsentr, Perm, 2001), issue 1, pp. 11–12 [in Russian].
8. V. A. Shabashov, S. V. Borisov, A. E. Zamatovskii, A. V. Litvinov, V. V. Sagaradze, and N. F. Vil'danova,

"Structural and phase transitions in nitrided layers of iron alloys during severe cold deformation," Bull. Russ. Acad. Sci.: Phys. **74**, 363–367 (2010).

9. V. A. Shabashov, K. A. Kozlov, K. A. Lyashkov, N. V. Kataeva, A. V. Litvinov, V. V. Sagaradze, and A. E. Zamatovskii, "Solid-state mechanical synthesis of austenitic Fe–Ni–Cr–N alloys," Phys. Met. Metallogr. **115**, 392–402 (2014).
10. V. A. Shabashov, L. G. Korshunov, V. V. Sagaradze, N. V. Kataeva, A. E. Zamatovsky, A. V. Litvinov, and K. A. Lyashkov, "Mössbauer analysis of deformation dissolution of the products of cellular decomposition in high-nitrogen chromium manganese austenite steel," Philos. Mag. **94**, 668–682 (2014).
11. V. A. Shabashov, S. V. Borisov, A. V. Litvinov, A. E. Zamatovsky, K. A. Lyashkov, V. V. Sagaradze, and N. F. Vildanova, "Mechanomaking of nanostructure in nitrided Fe-Cr alloys by cyclic "dissolution-precipitation" deformation-induced transformations," High Pressure Res. **33**, 795–812 (2013).
12. V. A. Shabashov, L. G. Korshunov, A. G. Mukoseev, V. V. Sagaradze, A. V. Makarov, V. P. Pilyugin, S. I. Novikov, and N. F. Vildanova, "Deformation-induced phase transitions in a high-carbon steel," Mater. Sci. Eng., A, 196–207 (2003).
13. E. P. Yelsukov and G. A. Dorofeev, "Mechanical alloying in binary Fe–M (M = C, B, Al, Si, Ge, Sn) systems," J. Mater. Sci. **39**, 5071–5079 (2004).
14. A. R. Kuznetsov, P. Yu. Butyagin, and I. K. Pavlychev, "Laboratory micromilling device for mechanochemical investigations," Prib. Tekh. Eksp. **6**, 201–204 (1986).
15. V. A. Shabashov, V. V. Sagaradze, A. V. Litvinov, and A. E. Zamatovskii, "Relaxation of the structure of Fe–Ni alloys during mechanical alloying induced by severe plastic deformation," Phys. Met. Metallogr. **116**, 869–875 (2015).
16. V. A. Shabashov, V. V. Sagaradze, A. E. Zamatovskii, V. P. Pilyugin, K. A. Kozlov, A. V. Litvinov, and N. V. Kataeva, "Dynamic aging in an Fe–Ni–Al alloy upon megaplastic deformation. Effect of the temperature and deformation rate," Phys. Met. Metallogr. **117**, 805–816 (2016).
17. V. V. Sagaradze, V. A. Shabashov, N. V. Kataeva, V. A. Zavalishin, K. A. Kozlov, A. R. Kuznetsov, A. V. Litvinov, and V. P. Pilyugin, "Deformation-induced dissolution of the intermetallics Ni_3Ti and Ni_3Al in austenitic steels at cryogenic temperatures," Philos. Mag. **96**, 1724–1742 (2016).
18. V. G. Gavriljuk and H. Berns, *High Nitrogen Steel: Structure, Properties, Manufacture, Applications* (Springer, Berlin, 1999).
19. V. S. Rusakov, *Mössbauer Spectroscopy of Locally Inhomogeneous Systems* (Izd-vo IYaF NYaTs, Almaty, 2000) [in Russian].
20. A. V. Makarov, S. N. Luchko, V. A. Shabashov, E. G. Volkova, A. L. Osintseva, A. E. Zamatovskii, A. V. Litvinov, and V. V. Sagaradze, "Structural and phase transformations and micromechanical properties of the high-nitrogen austenitic steel deformed by shear under pressure," Phys. Met. Metallogr. **118**, 53–64 (2017).
21. R. S. Reno and L. J. Swartzendruber, "Origin of Mössbauer linewidth in stainless steel," in *Magn. and Magn. Mater., 18th Ann. Conf. Denver., Colo., 1972.* Part 2 (New York, 1973), p. 1350.
22. B. P. Srivastava, H. N. K. Sarma, and D. L. Bhattacharya, "Ouadrupole splitting in deformed stainless steel," Phys. Status Solidi A **10** (2), K117–K118 (1972).
23. J.-M. R. Genin, "Mössbauer spectra analysis of Fe–N austenites," Scr. Metall. **24**, 399–402 (1990).
24. K. Oda, K. Umezu, and H. Ino, "Interaction and arrangement of nitrogen atoms in fcc γ iron," J. Phys.: Condens. Matter **2**, 10147–10158 (1990).
25. S. M. Dubiel and J. Zukrowski, "Mössbauer effect study of charge and spin transfer in Fe–Cr," J. Magn. Magn. Mater., **23**, 214–228 (1981).
26. V. A. Shabashov, A. L. Nikolaev, A. G. Mukoseev, V. V. Sagaradze, and N. P. Filippova, "Mössbauer spectroscopy of the thermal- and radiation-accelerated solid-solution decomposition in binary Fe–Cr alloys," Izv. Ross. Akad. Nauk., Ser. Fiz. **65,** 1010–1015 (2001).
27. V. A. Shabashov, K. A. Kozlov, K. A. Lyashkov, A. E. Zamatovskii, and S. G. Titova, "Deformation-intensified atomic separation in bcc Fe–Mn alloys," Phys. Met. Metallogr. **117**, 1210–1222 (2016).
28. S. G. Kang, H. Onodera, H. Jamamoto, and H. Watanabe, "Mössbauer effect study of Fe–Mn alloys," J. Phys. Soc. Jpn. **36**, 975–979 (1974).
29. H. J. Goldschmidt, *Interstitial Alloys* (Butterworths, London, 1967).
30. A. V. Makarov, L. G. Korshunov, V. M. Schastlivtsev, and N. L. Chernenko, "Wear resistance of nitrogen-containing high-chromium martensitic steels and structural changes in the surface layer of these steels under conditions of abrasive wear and sliding friction," Phys. Met. Metallogr. **86**, 400–407 (1998).
31. V. V. Sagaradze and V. A. Shabashov, "Anomalous diffusion phase transformations in steels upon severe cold deformation," Phys. Met. Metallogr. **112**, 146–164 (2011).
32. A. R. Kuznetsov and V. V. Sagaradze, "On the possible mechanism of low-temperature strain-induced dissolution of intermatallic phases in fcc Fe–Ni–Cr alloys," Phys. Met. Metallogr. **93**, 404–407 (2002).
33. V. A. Mogilevskii, V. V. Efremov, and I. O. Myshkin, "Behavior of a crystal lattice upon strong one-dimensional compression," Fiz. Goreniya Vzryva, No. 5, 750–754 (1977).
34. G. N. Epshtein, "Mass transfer in shock waves," in *High Pressures and Properties of Materials* (Naukova Dumka, Kiev, 1980), pp. 108–112 [in Russian].
35. A. N. Tyumentsev and I. A. Ditenberg, "Nanodipoles of partial disclinations as carriers of a quasi-viscous mode of deformation and of the formation of nanocrystalline structures upon severe plastic deformation of metals and alloys," Fiz. Mezomekh. **14** (3), 55–68 (2011).
36. P. Ehrhart, Atomic Defects in Metals, Landolt–Börnstein, New Series, Group III, Vol. 25, (Springer, New York, 1991), pp. 242–250.

Translated by O. Golosova